Materials Today Communications 42 (2025) 111448

Contents lists available at ScienceDirect

Materials Today Communications

journal homepage: www.elsevier.com/locate/mtcomm

Exploring the synergistic effects of Cu and Al_2O_3 reinforcements on nanoindentation and wear properties of aluminum based composite

Samuel Ranti Oke [a,c,*], Nthabiseng Maledi [a,b], Ismail Salaudeen [c], Oluwasegun Eso Falodun [a]

[a] School of Chemical and Metallurgical Engineering, Faculty of Engineering and the Built Environment University of the Witwatersrand, Johannesburg, South Africa
[b] DSI-NRF Centre of Excellence in Strong Materials, University of the Witwatersrand, Johannesburg, South Africa
[c] Department of Metallurgical and Materials Engineering, Federal University of Technology, Akure, Ondo State, Nigeria

ARTICLE INFO

Keywords:
Aluminium
Stir casting
Microstructure
Mechanical property
Wear

ABSTRACT

The study investigates the influence of hybrid reinforcements comprising aluminum oxide (Al_2O_3) and copper (Cu) on the microstructure, nanomechanical, and wear properties of aluminum-based composites. Six different compositions were prepared, including aluminum 6063 and composites with varying ratios of Al_2O_3 and Cu. Microstructural analysis via scanning electron microscopy (SEM) revealed a transition from a relatively homogeneous distribution in Al_2O_3-reinforced composites to a network-like structure with increasing Cu content due to phase segregation. Nanoindentation tests showed that composites with higher Al_2O_3 content exhibited superior hardness and elastic modulus, with sample S2 (75 wt% Al_2O_3 and 25 wt% Cu) demonstrating the highest nanohardness, stiffness and yield pressure. This composite also showed the lowest penetration depth and the highest load-carrying capacity, indicating enhanced resistance to plastic deformation. Wear tests revealed that composites with higher Al_2O_3 content exhibited lower wear rates, while increased Cu content reduced the coefficient of friction, enhancing tribological performance. The findings underscore the significance of optimizing Al_2O_3 and Cu ratios to achieve balanced mechanical properties and wear resistance in aluminum-based composites.

1. Introduction

The escalating demand for lightweight yet high-strength materials has positioned aluminum and its alloys at the forefront of modern engineering applications, notably within the aerospace and automotive sectors [1]. Aluminum's inherent low density, combined with its commendable physical, mechanical, and tribological properties, renders it an ideal candidate for numerous structural applications [2]. However, the intrinsic properties of monolithic aluminum often fall short in meeting the rigorous demands of specialized engineering applications, thereby catalyzing research into Aluminum Matrix Composites (AMCs) [3–5]. AMCs, characterized by the incorporation of reinforcing phases into the aluminum matrix, have demonstrated superior property combinations, such as enhanced specific strength, stiffness, and wear resistance, while maintaining satisfactory levels of corrosion resistance [6,7]. The strategic selection and integration of reinforcements can tailor these composites to exhibit desired properties. In particular, hybrid reinforcements, which employ multiple reinforcing agents, have gained traction due to their ability to synergistically improve mechanical and tribological performance [8]. Kumar et al. highlighted that hybrid composites exhibit elevated hardness, tensile strength, and wear resistance, alongside a reduced coefficient of friction, compared to their monolithic counterparts [9].

Within the realm of reinforcements, ceramic particulates such as silicon carbide (SiC) and aluminum oxide (Al_2O_3) have been extensively employed due to their high hardness and thermal stability [10,11]. Al_2O_3, or alumina, in its crystalline form, is not only pivotal in advanced ceramic applications but also serves as an effective reinforcement in AMCs, enhancing strength and specific stiffness. Nevertheless, challenges such as poor wettability and inherent porosity have impeded the optimal utilization of Al_2O_3 in composite fabrication [12,13]. To mitigate these issues, various processing methodologies have been explored, with stir casting emerging as a particularly efficacious technique [14]. Stir casting involves the incorporation of reinforcing particles into a molten metal matrix, achieved through mechanical stirring, ensuring uniform dispersion. This method stands out for its cost-effectiveness and

* Corresponding author at: School of Chemical and Metallurgical Engineering, Faculty of Engineering and the Built Environment University of the Witwatersrand, Johannesburg, South Africa.
E-mail addresses: okesam99@yahoo.com, samuel.oke@wits.ac.za (S.R. Oke).

https://doi.org/10.1016/j.mtcomm.2024.111448
Received 9 September 2024; Received in revised form 10 December 2024; Accepted 26 December 2024
Available online 27 December 2024
2352-4928/© 2024 The Author(s). Published by Elsevier Ltd. This is an open access article under the CC BY license (http://creativecommons.org/licenses/by/4.0/).

capability to produce large, near-net-shape components [15–17]. Empirical studies have validated the efficacy of stir casting in fabricating high-performance AMCs. For instance, Butola et al. demonstrated that aluminum-based hybrid composites produced via stir casting exhibited superior ultimate tensile strength (115.4 MPa), yield strength (76.4 MPa), and Vickers hardness (55–77 HV) relative to composites fabricated through alternative methods [18]. Similarly, Suryakumari et al. (2015) observed that the addition of 2.5 wt% Al_2O_3 and 5 wt% SiC via stir casting enhanced both hardness and impact strength in Al 7075 hybrid composites [19].

It is evident from literature that parameters such as the size, morphology, and volume fraction of reinforcements critically influence the mechanical properties of AMCs [20]. In this context, the incorporation of Cu as a secondary reinforcement alongside Al_2O_3 presents a promising avenue for property enhancement. Al_2O_3, with its high hardness and thermal stability, is expected to significantly improve the wear resistance and hardness of the composite [21]. Simultaneously, Cu plays a dual role; it not only enhances the mechanical strength through solid solution strengthening and precipitation hardening but also improves the thermal and electrical conductivity of the composite [22]. Previous studies have indicated that the addition of Cu in AMCs can lead to an increase in yield strength and tensile strength due to the formation of Cu-rich phases, which impede dislocation movement and enhance the load-bearing capacity of the matrix [23–26]. Moreover, Cu can also reduce the interfacial thermal mismatch between the matrix and ceramic reinforcements, thereby improving the overall thermal stability and wear resistance of the composite [27,28]. Thus, the synergistic effects of Cu and Al_2O_3 in the aluminum matrix are anticipated to yield a composite material with superior mechanical and tribological properties, making it suitable for advanced engineering applications.

Nanoindentation is a critical technique for evaluating the localized mechanical properties of AMCs, providing detailed insights into the effects of various reinforcements, particularly in terms of hardness and elastic modulus at the micro- and nanoscale [29,30]. The incorporation of hard ceramic particles like Al_2O_3 into AMCs has been shown to significantly enhance hardness, reduce plastic deformation under load, and improve wear resistance by minimizing material loss during sliding or abrasive conditions [17,31,32]. However, the synergistic effects of hybrid reinforcements, such as Al_2O_3 and Cu, on the microstructure-property relationships of AMCs remain underexplored. This work specifically addresses this knowledge gap by investigating the effects of these reinforcements on phase formation, microstructural evolution, and property optimization, with a focus on interactions such as Cu-induced precipitation hardening and interfacial strengthening.

This study systematically investigates the nanoindentation and wear properties of Cu/Al_2O_3 hybrid-reinforced AMCs, synthesized via the stir casting technique. By varying the proportions of Al_2O_3 and Cu reinforcements, the study elucidates their combined effects on the composite's microstructure, hardness, and tribological behavior. The novelty of this study lies in its systematic analysis of hybrid reinforcements in AMCs, providing new insights into the role of Cu in reducing interfacial thermal mismatch, enhancing precipitation hardening, and synergistically improving mechanical and tribological performance alongside Al_2O_3. This research aims to advance the understanding of hybrid reinforcement strategies in AMCs, contributing to their optimized application in demanding engineering environments.

2. Materials and method

2.1. Materials

The base materials for the investigation are Aluminium 6063, Copper (99.9 % purity), and Alumina. The morphology of the Al_2O_3 powder used in the experiment is angular, with an average particle size of 25 µm. Table 1 present the chemical compositions of the Aluminium 6063. Table 2 outlines the composition of six aluminum-based composite samples that were designed for casting. Sample 1 is Al alloy with no reinforcement, while the other five samples contain 10 wt% total reinforcement with varying ratios of Al_2O_3 to Cu. The ratios range from 1:0 (100 % Al_2O_3) to 0:1 (100 % Cu), with intermediate samples featuring mixed ratios like 3:1, 1:1, and 1:3. This design enables a detailed analysis of how different Al_2O_3 and Cu proportions affect the composite's properties.

2.2. Experimental procedures

The **aluminium alloy** was utilized as the metal matrix in this study, with copper particulates and Al_2O_3 powder selected as hybrid reinforcements to create aluminum-based composites. The composites were produced using a double stir casting process. Charge calculations determined the precise amounts of aluminum, Al_2O_3, and Cu needed to achieve a total reinforcement content of 10 wt%, with varying weight ratios of 1:0, 3:1, 1:1, 1:3, and 0:1. To enhance wettability and remove residual moisture, the Al_2O_3 particles were preheated separately to 250°C. Simultaneously, aluminum ingots were melted in a gas-fired crucible furnace, heated to 30°C above the liquidus temperature. Once fully liquefied, the molten Al alloy was cooled to approximately 600°C to reach a semi-solid state. At this point, the preheated Al_2O_3 particles were introduced into the matrix, followed by the addition of molten Cu. The slurry was manually stirred for 5 minutes to ensure initial dispersion of the reinforcements. Subsequently, the composite slurry was reheated to 720°C to ensure homogeneity and fluidity. A second stirring process was carried out using a mechanical stirrer at 300 rpm for 10 minutes, enhancing the uniform distribution of Al_2O_3 and Cu particles within the aluminum matrix. This controlled stirring process is essential for minimizing agglomeration and achieving a consistent microstructure. Finally, the well-mixed molten composite was cast into pre-prepared sand molds, solidifying the aluminum matrix composite with the desired hybrid reinforcement.

2.3. Microstructural characterization

The microstructure of the Al composites was examined using a JSM 7600 F JEOL ultra-high resolution field emission gun scanning electron microscope (FEG-SEM) equipped with an EDS for detailed

Table 2
Composition of aluminum-based composite samples with varying ratios of Al_2O_3 to Cu reinforcements.

Sample	Al wt%	Al_2O_3 (wt%)	Cu (wt%)	Al_2O_3 : Cu ration
S0	100	-	-	0:0
S1	90	10	-	1:0
S2	90	7.5	2.5	3:1
S3	90	5.0	5.0	1:1
S4	90	2.5	7.5	1:3
S5	90	-	10	0:1

Table 1
Chemical composition of aluminium 6063 alloy.

Elements	Si	Fe	Cu	Mn	Mg	Zn	Cr	Ti	Al
Composition (%)	0.45	0.22	0.02	0.03	0.5	0.02	0.03	0.02	Bal

microstructural analysis and elemental composition determination. Prior to analysis, the samples were prepared to ensure optimal surface integrity. A semi-automated metallographic sample preparation system (Advanced Laboratory Solutions, ATM Saphir 550) was used for grinding and polishing the samples. The final polishing stage employed a 0.2 μm colloidal fumed silica suspension to achieve a mirror-like surface finish. After polishing, the samples were cleaned with acetone and air-dried, ensuring they were ready for microstructural and compositional investigations.

2.4. Nanoindentation testing

The mechanical properties of the Al composites were evaluated using an ultra nanoindenter (UNHT) from Anton Paar, Switzerland, equipped with a Berkovich diamond indenter, following ISO 14577 standards. Nanoindentation was carried out on flat, polished surfaces of the samples at applied loads of 50 and 100 mN, with a loading rate of 10 mN/min. For each load, a minimum of 15 indentations were performed per sample, with a pause time of 1000 s between indentations to mitigate viscoelastic effects and assess time-dependent deformation. The hardness (H) and reduced elastic modulus (Er) were determined from the load-displacement data using the Oliver and Pharr method [33], with hardness calculated as the ratio of maximum load (P_{max}) to the projected contact area (Ac) as presented in Eq. 1.

$$H = \frac{P_{\max}}{Ac} \tag{1}$$

The Er is calculated as expressed in Eq. 2, which relates it to the Poisson's ratio of the sample (Vs) and the indenter (Vi), as well as the elastic modulus of the sample (Es) and the indenter (Ei).

$$\frac{1}{E_r} = \frac{1 - v_s^2}{E_s} + \frac{1 - v_i}{E_i} \tag{2}$$

The total work done by the indenter (W_t) is used to evaluate the elastic recovery index (W_e/W_t) and the plasticity index (W_p/W_t), which characterize the mechanical behavior of the Al composites. The total work W_t is the sum of the plastic work W_p and the elastic work W_e.

2.5. Wear testing of Al composite

Wear testing of the aluminum composite samples was performed using an Anton Paar tribometer configured for a ball-on-disc wear testing setup. The samples, mechanically polished to a smooth surface finish, were subjected to dry sliding wear testing at ambient temperature. The test parameters were as follows: a duration of 1800 s, an applied normal load of 10 N, and a total sliding distance of 115 m. The radius of the wear track was 2.41 mm, the linear sliding speed was 6.31 cm/s, and the data acquisition rate was set to 10 Hz. The coefficient of friction (COF) was obtained during the test, and wear volume and wear rates were calculated. The wear volume (V_w) was determined using the formula:

$$V_W = \frac{m}{\rho} \qquad \text{Eq. 3}$$

where m is the mass loss of the sample and ρ is the density of the material. The wear rate (WR) was calculated using:

$$WR = \frac{V_W}{\text{F.d}} \qquad \text{Eq. 4}$$

where F is the applied load and d is the sliding distance. The wear test results, including COF, wear volume, and wear rates, were analyzed to evaluate the wear resistance of the composites. The tests were conducted for each composite variant to ensure the reliability and reproducibility of the results. Each test was repeated three times under identical conditions, and the results were consistent, with deviations in mean CoF values observed to be minimal across the trials. This reproducibility highlights the robustness of the experimental setup and the reliability of the observed trends

3. Results and discussion

3.1. Microstructural characterization

The microstructural evolution of the Al 6063-based composites depicted in Fig. 1 highlights the distinct roles of Al_2O_3 and Cu in modifying the matrix morphology and grain boundary characteristics. In the unreinforced Al 6063 (S0), the microstructure consists predominantly of equiaxed α-Al grains, typical of the alloy after solidification. The absence of secondary phases or reinforcements in S0 leads to limited grain boundary delineation. Upon the introduction of 10 wt% Al_2O_3 in S1, a pronounced dispersion of Al_2O_3 ceramic particles is observed. These particles serve as nucleation sites during solidification, promoting heterogeneous nucleation and refining the grain structure. Studies by Oke et al. [34] confirm that addition of Al_2O_3, enhances grain refinement by reducing grain boundary mobility and acting as pinning points during recrystallization. In the hybrid composites, the introduction of Cu in addition to Al_2O_3 results in more complex microstructural features. In S2 and S3, where Cu content ranges from 2.5 to 5 wt%, Cu-rich phases are observed along grain boundaries, accompanied by dispersed Al_2O_3 particles within the matrix. This dual-phase interaction creates a microstructure with distinct grain boundary reinforcement. The Cu phases at boundaries are indicative of eutectic reactions during solidification, as supported by findings from Han et al. [35], who noted similar Cu-segregated phases in Al-Cu composites, attributing them to localized enrichment during cooling. The Al_2O_3 particles in these composites remain well-distributed and maintain their role in grain refinement, as confirmed by their consistent morphology and location within the α-Al grains.

At higher Cu concentrations, as in S4 (7.5 wt% Cu), the microstructure undergoes significant changes with increased interconnectivity of Cu-rich phases along the grain boundaries. These continuous boundary features suggest coalescence of Cu during solidification, a phenomenon reported by Ghoncheh et al. [36] in Al-Cu composites, where Cu enrichment promotes phase segregation at grain boundaries due to reduced solubility at lower temperatures. In S5, comprising Cu, the microstructure lacks the ceramic reinforcement of earlier samples, resulting in larger and more distinct Cu grains separated by Cu-rich boundaries. The transition from dispersed particles (S1-S3) to interconnected networks (S4-S5) underscores the role of Cu in altering the grain boundary morphology, with Al_2O_3 maintaining its influence primarily within the earlier stages of hybrid reinforcement. These observations align with recent advancements in the development of hybrid composites, emphasizing the complementary roles of ceramic and metallic additions in tailoring microstructural characteristics [18].

The EDS as depicted in Fig. 2 confirms the presence of Cu-rich regions along the grain boundaries, as highlighted in the microstructure. The EDS spectrum demonstrates a significant intensity of Cu peaks, corroborating the elemental composition of the regions examined. The accompanying SEM image illustrates the Cu-rich phases that predominantly decorate the grain boundaries, forming continuous or semi-continuous networks. This aligns with the earlier observation of Cu segregation in hybrid Al 6063 composites with higher Cu concentrations, emphasizing the role of Cu in boundary enrichment. The presence of Cu at these boundaries is indicative of a eutectic or phase segregation phenomenon, as noted by Han et al. [35], where Cu preferentially migrates and solidifies at the grain boundaries during cooling due to limited solubility in the Al matrix at room temperature. This compositional evidence further validates the hypothesis that Cu additions not only reinforce grain boundaries but also significantly alter their morphology, transforming them into Cu-rich pathways that impact the overall grain structure. Additionally, the minimal presence of other

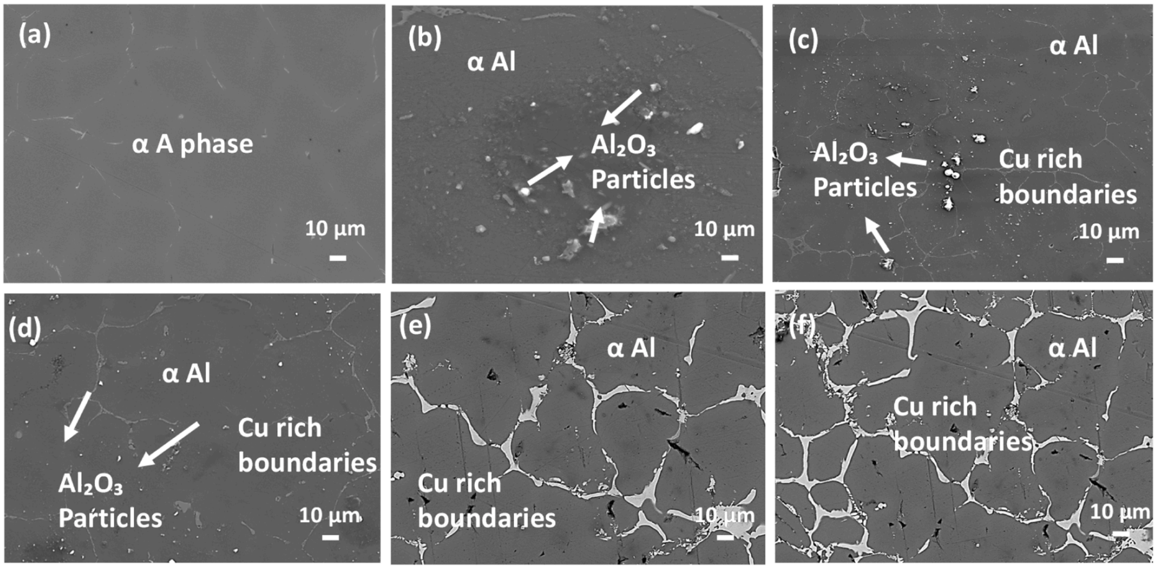

Fig. 1. (a-f): SEM images of (a) S0, Al 6063, (b) S1, Al 6063 with 10 wt% Al_2O_3 (c) S2, Al 6063 with 7.5 wt% Al_2O_3 and 2.5 wt% Cu (d) S3, Al 6063 with 5 wt% Al_2O_3 and 5 wt% Cu (e) S4, Al 6063 with 2.5 wt% Al_2O_3 and7.5 wt% Cu (f) S5, Pure Cu, composite samples.

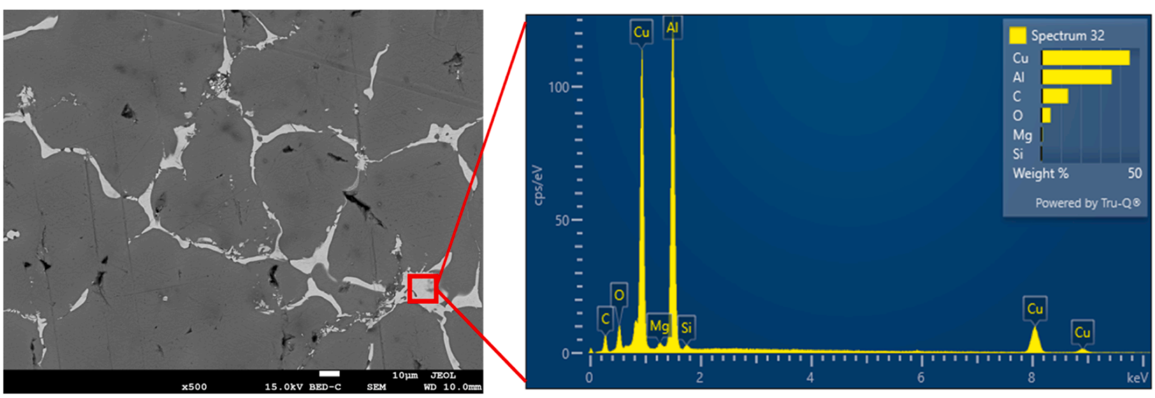

Fig. 2. SEM image of the Al 6063 composite (S4) with EDS confirming Cu-rich grain boundaries through prominent Cu peaks, highlighting significant Cu enrichment at intergranular regions.

elements such as Mg and Si in the spectrum suggests that the Cu-rich phases are relatively pure, consistent with studies by [37–39], which reported similar microstructural features in Al-Cu systems.

The EDS spectra (Fig. 3) for samples S0 to S5 highlight variations in elemental composition that correspond to the reinforcement content. In S0, the dominant Al peak is accompanied by Mg and Si peaks, which are alloying elements in the Al matrix. The presence of O in S0 likely results from surface oxidation, while the C peak is attributed to surface contamination. As Al_2O_3 is introduced in S1, the O peak increases significantly, confirming the presence of the ceramic oxide. With the progressive addition of Cu in S2 to S5, Cu peaks emerge and intensify, reflecting the increasing Cu content. For instance, S2, with 25 % Cu, shows a moderate Cu peak, whereas S5, with 100 % Cu, exhibits a dominant Cu peak, accompanied by a decrease in O content as Al_2O_3 decreases. This trend indicates that as Cu replaces Al_2O_3 in the composite, the oxygen content reduces due to the lower oxide phase. The consistent presence of Mg and Si across all samples aligns with their role as alloying elements in the Al matrix, while trace elements like Mn and Ca appear in the Cu-containing samples, possibly introduced during the processing or as minor alloying elements.

3.2. Nanoindentation studies of the mechanical properties of composite samples

The nanoindentation testing technique was used to evaluate the nanohardness, elastic modulus, elastic recovery index, resistance to elastic strain to failure, and the yield pressure and the plasticity index of the composite samples. In addition, the load-depth and displacement-time plots were used to assess the mechanical behaviour of the samples in this section.

3.2.1. Elastic-plastic response during loading and unloading of the Al composites

Fig. 4 presents the load-displacement curves obtained during nanoindentation testing of the Al composites at two different applied loads of 50 mN and 100 mN for the samples: Al 6063 (S0), Al reinforced with Al_2O_3 (S1), Al reinforced with 75 % Al_2O_3 and 25 % Cu (S2), Al reinforced with 50 % Al_2O_3 and 50 % Cu (S3), Al reinforced with 25 % Al_2O_3 and 75 % Cu (S4), and Al reinforced with 100 % Cu (S5). The loading curves for all samples show an increase in penetration depth with applied load, with Al 6063 (S0) consistently exhibiting the greatest depth. This indicates that S0 undergoes more plastic deformation compared to the reinforced samples. As the content of Al_2O_3 and Cu increases, the penetration depth decreases, showing that these

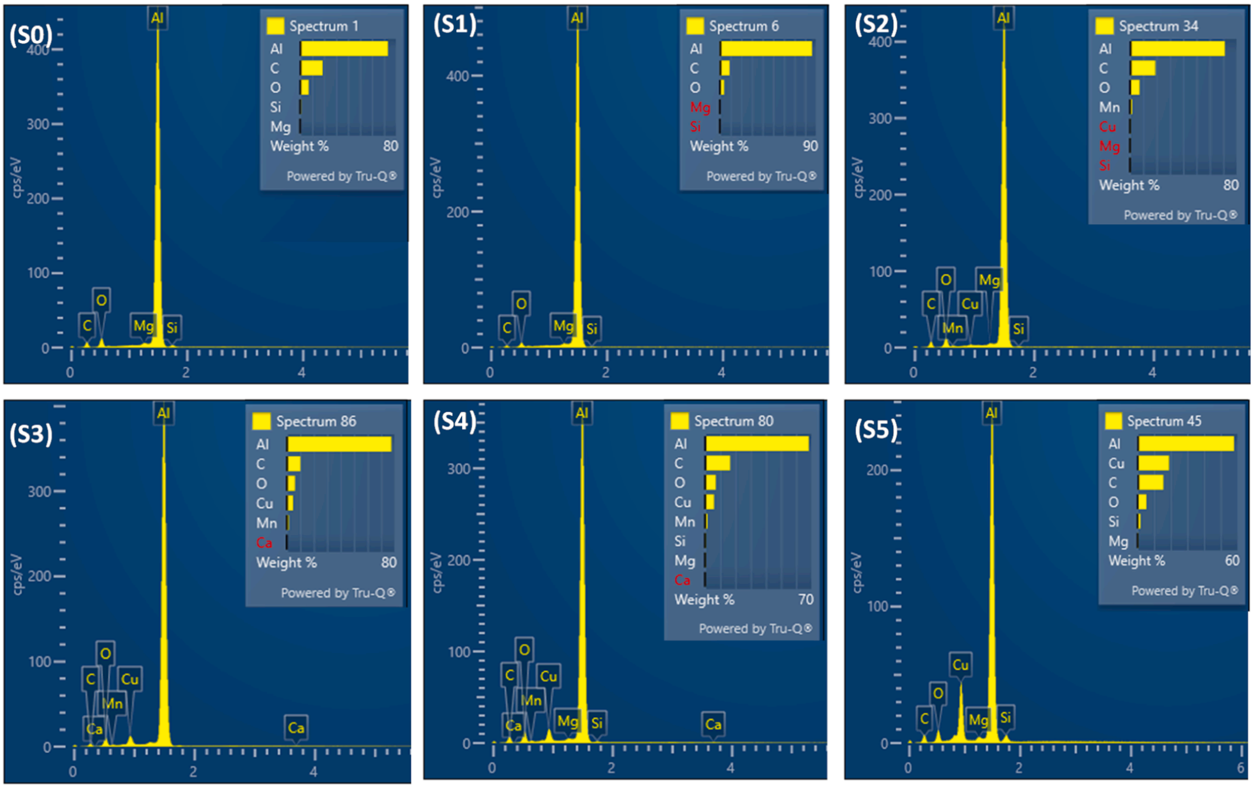

Fig. 3. EDS spectra of samples S0 to S5, illustrating the elemental composition for each sample based on the varying reinforcement content.

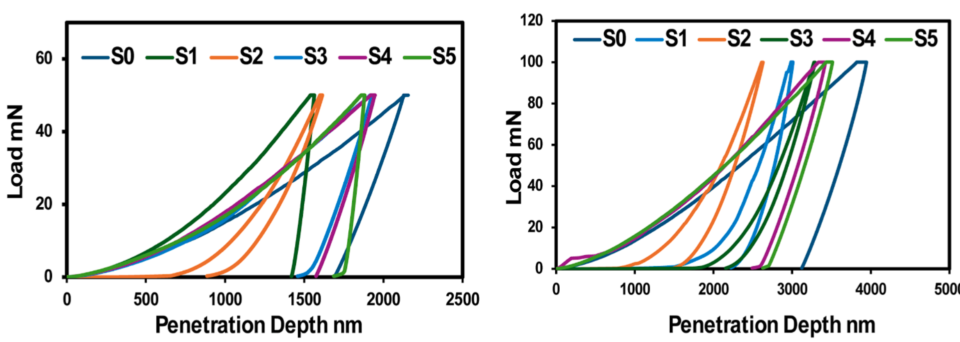

Fig. 4. Load penetration depth curve depicting the elastic-plastic response of the composite under indentation load (a) 50mN, (b) 100mN respectively.

reinforcements contribute to reducing plasticity under the applied loads. The steeper loading curves observed for the samples with higher reinforcement content (S1 and S2) suggest a greater resistance to penetration, pointing to a more elastic response during loading. The unloading curves reveal the elastic recovery behavior of each sample. In both figures, it is evident that the samples with higher reinforcement content, particularly those with a higher Al_2O_3 ratio (S1 to S4), exhibit less residual depth upon unloading. This reduced residual depth indicates a greater proportion of elastic recovery, suggesting that the elastic strain energy stored during loading is more effectively recovered [40]. This behavior affirms that hard, stiff reinforcements could exhibit enhanced resistance to both plastic deformation and elastic recovery, as the hard particles act as barriers to dislocation motion [41,42]. Conversely, Al (S0) shows the least elastic recovery, with a higher residual indentation depth, indicating a predominantly plastic deformation during the indentation process. This behavior underscores the role of reinforcements in enhancing the elastic-plastic response of the composites.

3.2.2. Load carrying capacities due to penetration depth with time

Fig. 5(a-b) presents the penetration depth of the indenter as a function of time for samples S0 to S5 under indentation loads of 50 mN and 100 mN, serving as a direct measure of their load-carrying capacities. S0 (Al 6063) exhibits the greatest penetration depth across both loads, underscoring its limited load-carrying capacity due to the absence of reinforcing phases. The material's lower hardness allows for more significant deformation under applied stress, leading to deeper penetration. Composite sample 75 wt% Al_2O_3 and 25 wt% Cu (S2) demonstrates the shallowest penetration depth, indicating the highest load-carrying capacity among the composites. The higher Al_2O_3 content provides enhanced resistance to the indenter, thereby minimizing penetration and signifying superior mechanical strength [43]. S1 (100 % Al_2O_3) also exhibits a shallow penetration depth, slightly greater than S2, due to the absence of Cu, which might offer additional toughness but at the cost of increased penetration. The hybrid composites S3, S4, and S5 display increasing penetration depths with higher Cu content. This trend reflects the reduction in load-carrying capacity as Cu's more ductile nature allows for greater deformation under the same applied load [44],

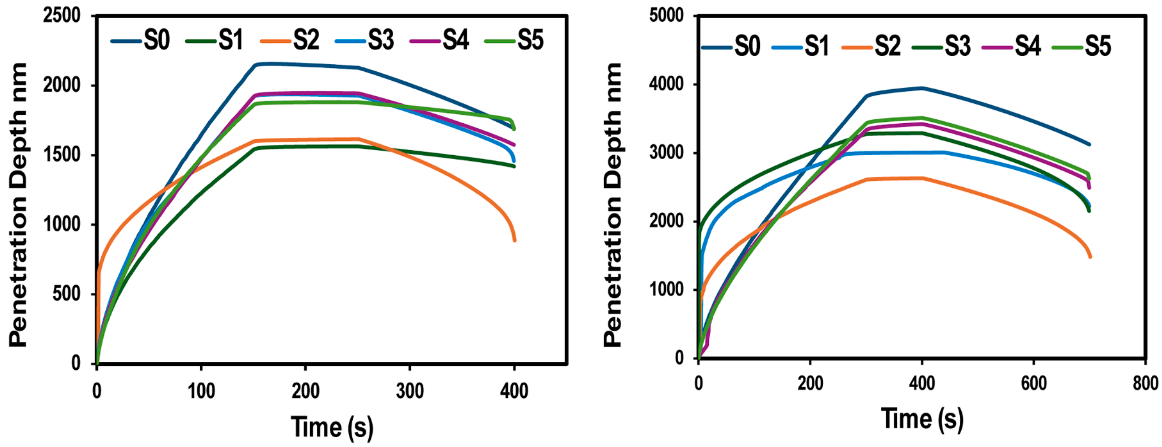

Fig. 5. Penetration depth of indentation with time curves depicting the load carrying capacities of the composite under indentation load (a) 50mN, (b) 100mN respectively.

compared to the harder Al_2O_3 particles. The results clearly indicate that S2's optimized balance of Al_2O_3 and Cu maximizes load-carrying capacity by harnessing the hardness of Al_2O_3 and the toughening effect of Cu.

3.2.3. Nanohardness and reduced elastic modulus of the samples

The nanohardness results in Fig. 6 reveal that the composite S2 (Al with 7.5 wt% Al_2O_3 and 2.5 wt% Cu) exhibits the highest nanohardness values, approximately 1171 MPa at 50 mN and 897 MPa at 100 mN. This superior hardness can be attributed to the microstructural characteristics observed in S2, particularly the presence of a refined dendritic structure coupled with the uniform distribution of Al_2O_3 particles. The dendritic structure of the aluminum matrix, which forms during solidification, provides a framework that resists deformation, while the dispersed Al_2O_3 particles act as pinning sites that obstruct dislocation motion, leading to enhanced hardness [45–47]. The effectiveness of the Al_2O_3 particles in reinforcing the matrix is particularly evident in S2, where their optimal content, combined with a small amount of Cu, improves the load transfer between the matrix and the reinforcement. This synergistic effect is consistent with the findings of [48,49], who observed that a balanced combination of ceramic and metallic reinforcements can significantly enhance the mechanical properties of metal matrix composites. Conversely, samples with higher Cu content, such as S4 (2.5 wt% Al_2O_3 and 7.5 wt% Cu) and S5 (pure Cu), show reduced hardness, with values around 663 MPa and 630 MPa at 50 mN, respectively. This decrease is attributed to the relatively softer nature of Cu, which does not contribute as effectively to the obstruction of dislocations compared to the hard Al_2O_3 particles. Additionally, the decrease in hardness with increasing load across all samples suggests greater plastic deformation under higher applied forces, which is a typical characteristic of indentation in composites.

The elastic modulus results in Fig. 7 reveal that sample S2 (Al with 7.5 wt% Al_2O_3 and 2.5 wt% Cu) exhibits the highest stiffness, with values reaching approximately 94 GPa at 50 mN and 83 GPa at 100 mN. This superior stiffness can be attributed to the high stiffness of the Al_2O_3 reinforcing phase, which has a stiffness of around 380 GPa, significantly enhancing the composite's resistance to elastic deformation. The presence of Al_2O_3 in S2 contributes to this high modulus by acting as a stiffening agent, a phenomenon supported by studies that have shown the effectiveness of Al_2O_3 in improving the elastic modulus of Al-based composites [50]. In contrast, S1 (Al with 10 wt% Al_2O_3) has slightly lower stiffness values of about 83 GPa at 50 mN and 71 GPa at 100 mN, reflecting the influence of the Al matrix, which has a much lower stiffness of approximately 70 GPa, and the absence of Cu, which also possesses a relatively low stiffness (~110 GPa). On the other hand, samples S4 and S5 (pure Cu) display even lower stiffness, with elastic moduli around 77 GPa and 72 GPa at 50 mN, respectively, likely due to the higher Cu content reducing the overall stiffness of the composite. These results align with previous studies [17,51] that indicate the addition of high stiffness reinforcing phases like Al_2O_3 significantly boosts the elastic modulus of metal matrix composites, while higher concentrations of softer materials like Cu can reduce it. The observed trend of decreasing elastic modulus with increasing load across all samples may be due to the reduced elastic recovery under higher indentation loads, a behavior consistent with findings in other composite systems [52].

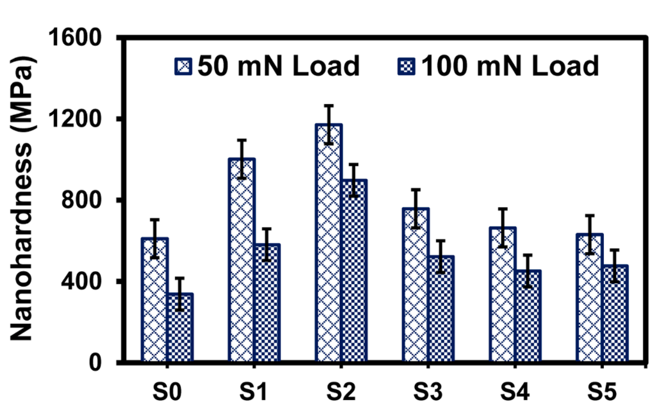

Fig. 6. Variation in nanohardness values of the composites (S0 to S5) under indentation loads of 50 mN, 100 mN respectively.

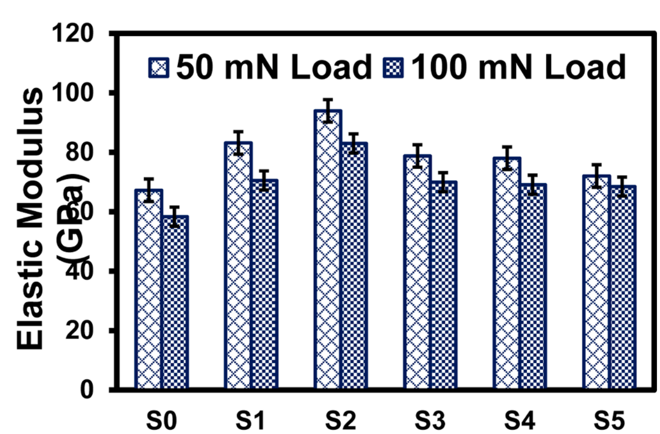

Fig. 7. Variation in Reduced elastic modulus values of the composites (S0 to S5) under indentation loads of 50 mN, 100 mN respectively.

3.2.4. Mechanical and anti-wear behaviours of the samples

The hardness to elastic modulus ratio (H/Er) is a critical parameter that reflects the wear resistance of materials, where a higher H/Er ratio typically indicates better resistance to wear. Fig. 8 shows that sample S2 (Al with 7.5 wt% Al_2O_3 and 2.5 wt% Cu) exhibits the highest H/Er ratio, with values of approximately 0.012 at 50 mN and 0.010 at 100 mN. This superior ratio can be attributed to the combined effect of the hard Al_2O_3 particles, which contribute to a high hardness, and the moderate stiffness provided by the Cu phase, enhancing the overall wear resistance of the composite. On the other hand, sample S5 (pure Cu) shows the lowest H/Er ratio, about 0.006 at both loads, due to the lower hardness of copper and its relatively lower stiffness (around 110 GPa), which allows more plastic deformation under similar conditions. The observed trend where the H/Er ratio decreases slightly with increasing load across all samples can be linked to the increased dominance of elastic deformation under higher loads. This results in a reduced ability to resist wear, as the material becomes more susceptible to plastic deformation. These findings suggest that incorporating hard, stiff reinforcing phases like Al_2O_3 into a metal matrix is essential to improving wear resistance, which is consistent with the theoretical principles of material design and supported by previous research on metal matrix composites [31,53].

Yield pressure, often represented by the ratio H^3/Er^2, is a critical parameter that reflects the resistance of a material to plastic deformation under an applied load. This ratio is significant because it provides insights into the material's strength relative to its elastic properties, making it an essential factor in applications requiring high load-bearing capacity. In Fig. 9, the yield pressure of the different samples under both 50 mN and 100 mN loads is presented. The S2 sample, exhibits the highest yield pressure values, approximately 0.0045 and 0.0042 at 50 mN and 100 mN loads, respectively. This suggests that S2 possesses the greatest resistance to plastic deformation and ability to withstand higher pressures without yielding among the samples, likely due to the optimal distribution and synergistic interaction between the Al_2O_3 particles and Cu reinforcement. The S1 sample, containing 10 wt% Al_2O_3, also shows relatively high yield pressure values, around 0.0043 and 0.0017 for 50 mN and 100 mN loads, respectively, which highlights the effectiveness of Al_2O_3 in reinforcing the aluminum matrix. However, the slightly lower values compared to S2 may be attributed to the absence of Cu, which could have otherwise provided additional strengthening through mechanisms such as solid solution strengthening and precipitation hardening. On the other hand, samples S3, S4, and S5, which contain higher proportions of Cu, show a decrease in yield pressure, with S5 exhibiting the lowest values at approximately 0.001. This reduction in yield pressure for samples with higher Cu content could be due to the lower inherent hardness and elastic modulus of Cu compared to Al_2O_3, which diminishes the overall resistance to plastic deformation.

The plasticity index (ψ) is a crucial parameter that quantifies the extent to which a material undergoes plastic deformation relative to its elastic deformation under an applied load. This index is particularly relevant in evaluating the ductility and toughness of materials, as it directly influences their ability to absorb energy before failure. A higher plasticity index indicates greater plastic deformation capacity, which is essential in applications where materials must withstand significant deformation without fracturing. In the analysis of the ψ for the samples subjected to 50 mN and 100 mN loads, as depicted in Fig. 10, a notable trend emerges. Sample S0, representing the unreinforced aluminum matrix, displays the highest ψ values of approximately 0.43 and 0.45 for 50 mN and 100 mN loads, respectively. This indicates that the aluminum alloy matrix has the greatest capacity for plastic deformation, which aligns with the inherent ductility of aluminum as a base metal. The absence of reinforcing phases allows for more extensive plastic deformation, resulting in higher ψ values.

Conversely, the introduction of reinforcements, particularly in the S1 and S2 samples, leads to a marked reduction in plasticity index values. S2, which contains 7.5 wt% Al_2O_3 and 2.5 wt% Cu, exhibits ψ values of approximately 0.09 and 0.17 at 50 mN and 100 mN loads, respectively. The presence of hard Al_2O_3 particles restricts the extent of plastic deformation by increasing the overall stiffness and reducing the ductility of the composite. This behavior is consistent with the findings of previous studies, where the addition of ceramic reinforcements like Al_2O_3 in AMCs significantly lowers the plasticity index due to the reduced ability of the material to undergo plastic deformation [54,55]. Interestingly, the ψ tends to increase again in samples with higher Cu content, such as S4 and S5. The S5 shows ψ values of approximately 0.25 and 0.38 at 50 mN and 100 mN loads, respectively. This can be attributed to the

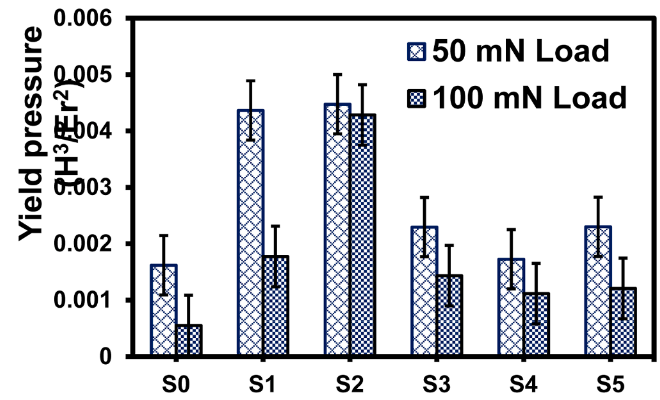

Fig. 9. Variation in yield pressure depicting the resistance to plastic deformation of the composites (S0 to S5) under indentation loads of 50 mN, 100 mN respectively.

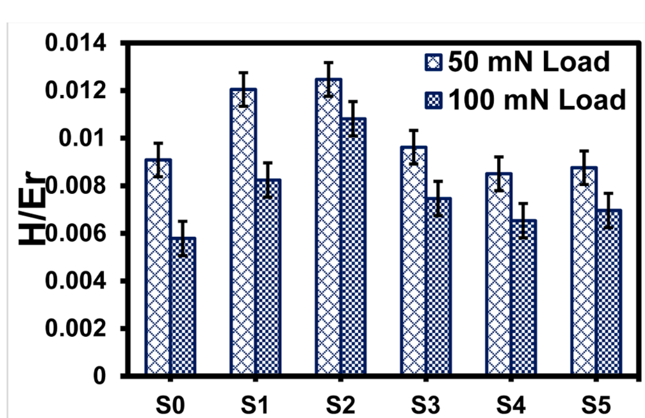

Fig. 8. Variation in H/Er ratio depicting the anti-wear resistance of the composites (S0 to S5) under indentation loads of 50 mN, 100 mN respectively.

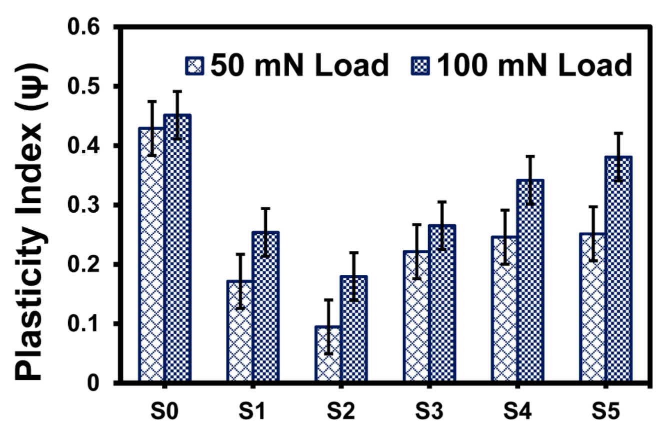

Fig. 10. Variation in the plasticity index (ψ) of the composites (S0 to S5) under indentation loads of 50 mN, 100 mN respectively.

inherent ductility of copper, which, when added in higher proportions, compensates for the reduced plasticity introduced by the Al_2O_3 particles. Cu's ability to enhance plastic deformation aligns with its mechanical properties, contributing to a moderate increase in the plasticity index compared to samples with lower Cu content [56].

3.3. Wear properties of Al alloy and composites

The coefficient of friction (CoF) is a critical parameter in evaluating the tribological performance of materials, particularly in wear applications. Fig. 11 (a & b) illustrates the CoF variation over time and the mean CoF values for different aluminum matrix composites under a 10 N load. As observed from the figure, the samples recorded high coefficient of friction at the beginning of the wear test, but subsequently decreases and stabilizes. This can be attributed to the initial running-in phase of the tribological test. During this phase, surface asperities on the sample and the counterface come into direct contact, leading to higher friction due to localized stress and wear. As the process continues, the asperities are gradually worn down, and a more stable tribological interface forms, often aided by the generation of wear debris or tribolayers. In the case of Cu-containing composites (S4 and S5), the formation of a Cu-rich tribolayer likely contributes to the stabilization and reduction of the CoF over time, while in Al_2O_3-reinforced composites, the hard particles help maintain surface integrity and minimize fluctuations in friction. The unreinforced sample (S0) exhibits the highest mean CoF of approximately 0.52, indicating greater resistance to sliding motion, likely due to the lack of hard reinforcements that could otherwise reduce surface interaction. In contrast, samples S4 and S5, which have higher Cu content, show significantly lower mean CoF values of around 0.44, suggesting that the introduction of Cu enhances the self-lubricating properties of the composite, possibly due to the formation of a Cu-rich tribolayer that reduces friction [57].

The intermediate CoF values observed in S1, S2, and S3, which range between 0.47 and 0.49, can be attributed to the combined effects of Al_2O_3 and Cu reinforcements. The presence of hard Al_2O_3 particles likely contributes to increased surface hardness, reducing material deformation and wear. However, without the optimal balance of Cu, as seen in S4 and S5, the CoF does not decrease as significantly. This observation aligns with studies by [17], who reported that hybrid composites containing a balanced mixture of hard and soft reinforcements tend to exhibit lower friction coefficients due to improved load distribution and the formation of protective surface films during sliding.

Fig. 12 (a & b) presents the variation in wear volume and wear rate for the different AMCs under a 10 N load. The results clearly indicate that the wear volume and wear rate increase as the Cu content in the composite increases, while they decrease with higher Al_2O_3 content. Al 6063 (S0) exhibits the highest wear volume (1.4×10^{-3} mm^3) and wear rate (2.2×10^{-7} mm^3/Nm), indicative of its relatively poor wear resistance compared to the reinforced samples. The single-reinforced Al_2O_3 sample (S1) shows the lowest wear volume (5.1×10^{-3} mm^3) and wear rate (2.2×10^{-8} mm^3/Nm), demonstrating the superior wear resistance imparted by the Al_2O_3 particles. This behavior aligns with the well-established theory that hard ceramic reinforcements like Al_2O_3 improve wear resistance by providing a barrier to material removal and reducing the direct contact between the matrix and the abrasive counterface [58,59]. As Cu content increases in the composites (S2 to S5), the wear volume and wear rate increased, with S5 (100 % Cu) showing a wear volume of 1.4×10^{-3} mm^3 and a wear rate of 2.1×10^{-8} mm^3 /Nm. This increase in wear can be attributed to the relatively lower hardness of Cu compared to Al_2O_3, which leads to greater material removal during sliding wear conditions. The combination of Al_2O_3 and Cu in hybrid composites (S2 to S4) reveals a trade-off between hardness and toughness, where increased Cu content enhances the composite's ductility but compromises its wear resistance due to lower hardness.

Fig. 13 shows SEM images of the wear tracks for samples S0 to S5, illustrating how the wear mechanisms and surface features vary with the type and proportion of reinforcement. S0 exhibits a smooth wear track with deep grooves, indicating severe abrasive wear due to the absence of reinforcement particles, which makes it susceptible to plowing and material removal. In contrast, the composite containing only Al_2O_3 as the reinforcement (S1) displays a much finer wear track with shallow grooves, suggesting that the hard Al_2O_3 particles effectively resist plowing and abrasive wear, thereby improving wear resistance. As the Cu content in the hybrid composites increases progressively from S2 to S5, the wear tracks exhibit increasingly pronounced plastic deformation and delamination, particularly in the composite with 25 % Al_2O_3 and 75 % Cu reinforcement (S4) and the composite with only Cu as the reinforcement (S5), where the wear mechanism shifts predominantly towards adhesive wear. This shift is due to the ductile nature of Cu, which promotes material transfer and adhesion to the counterface, resulting in higher wear volumes and more significant material loss. The comparison between these samples highlights the critical role of Al_2O_3 in enhancing wear resistance through its hardness and ability to resist deformation, while the increasing Cu content reduces the composite's hardness, leading to a dominance of adhesive wear mechanisms.

3.4. Microstructure-property relationships in Al 6063 composites

The microstructural evolution of Al 6063 composites, driven by the addition of Al_2O_3 and Cu, plays a pivotal role in defining their mechanical and tribological properties. The incorporation of Al_2O_3 leads to significant grain refinement, as observed in the SEM images of S1, S2, and S3. The Al_2O_3 particles act as nucleation sites during solidification, increasing the grain boundary density and impeding dislocation motion, resulting in enhanced yield strength and hardness. However, due to their size (~25 μm), Al_2O_3 particles primarily contribute to load transfer and thermal mismatch (CTE difference) effects rather than interacting with dislocations via the Orowan mechanism. This refinement effect is

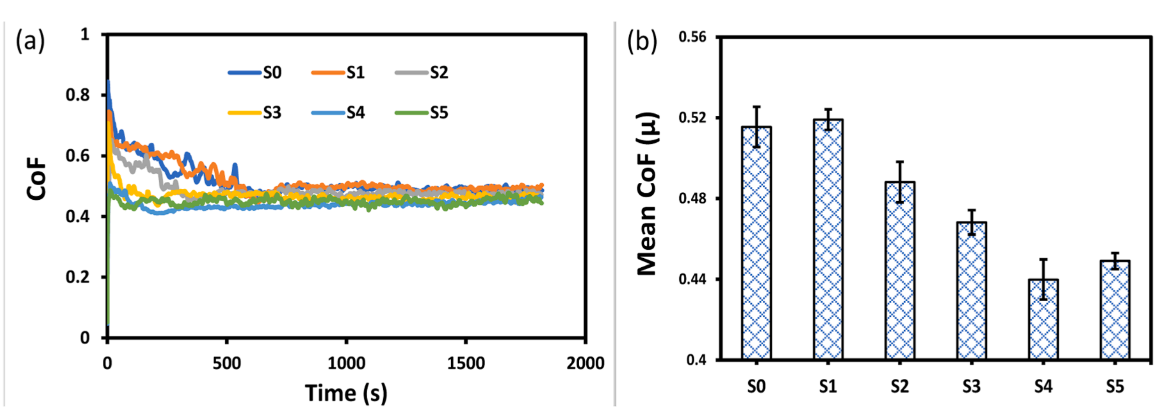

Fig. 11. Variation in (a) coefficient of friction, CoF and (b) estimated mean CoF of the composites (S0 to S5) under 10 N load.

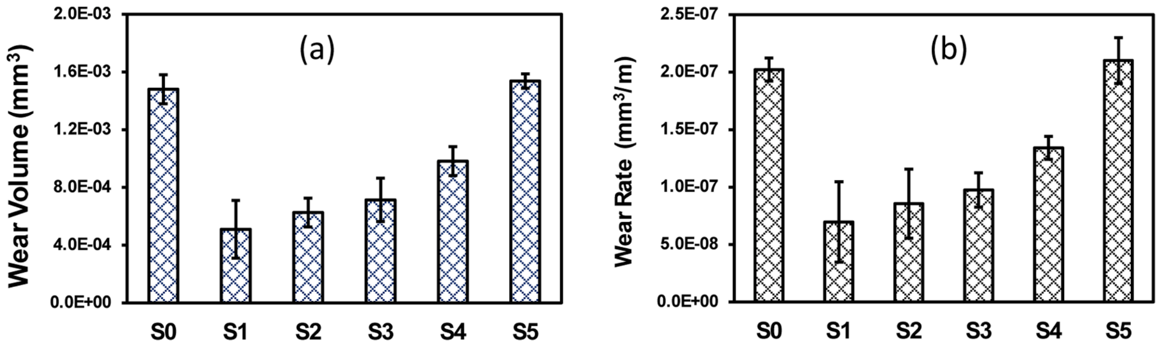

Fig. 12. Variation in estimated (a) wear volume and (b) wear rate of the composites (S0 to S5) under 10 N load.

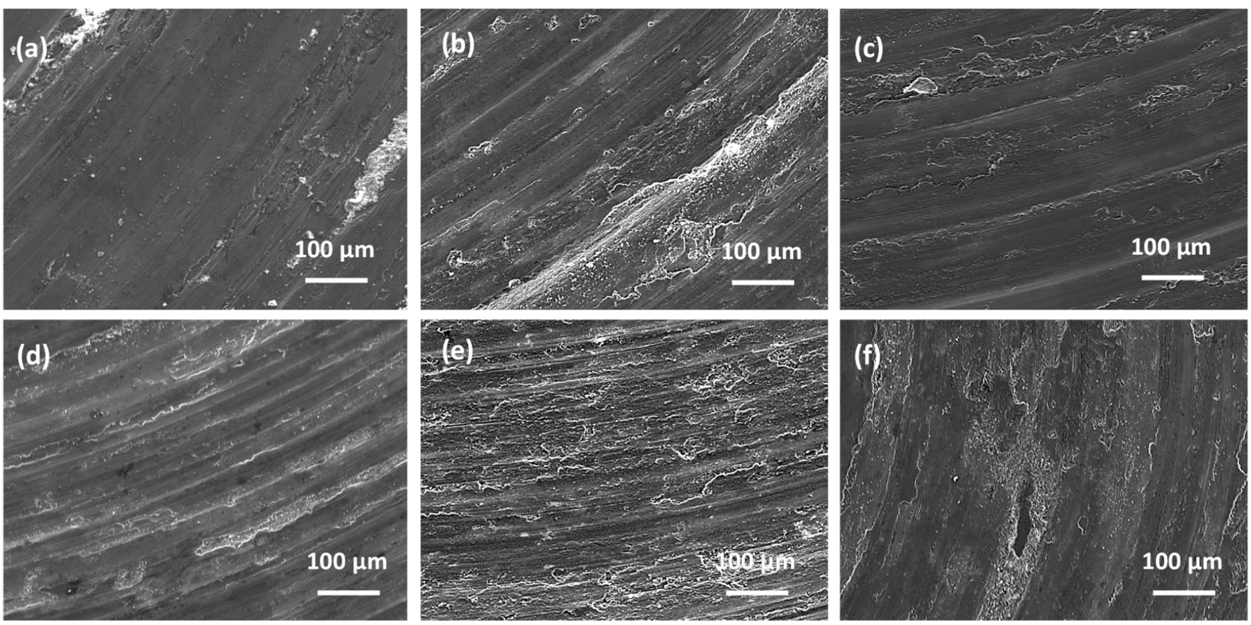

Fig. 13. Microstructural analysis of the wear track morphologies of the composites (S0 to S5) under 10 N load.

reflected in the improved hardness and reduced plasticity indices of composites with higher Al_2O_3 content, such as S2. Conversely, the grain refinement effect diminishes in composites with lower Al_2O_3 content, such as S4, where the microstructure is dominated by Cu-rich phases, reducing the overall grain boundary area.

The addition of Cu introduces Cu-rich phases along the grain boundaries, as confirmed by EDS in Fig. 2. These phases, formed during solidification, enhance matrix reinforcement by restricting grain boundary sliding and dislocation motion. However, the potential for precipitation hardening in Cu-containing composites is also considered. The cooling rate during solidification directly affects Cu solubility in the aluminum matrix and the formation of precipitates such as θ-phase (Al_2Cu). Composites with higher Cu content (e.g., S4 and S5) exhibit a reduction in hardness and elastic modulus due to the overconnectivity of Cu-rich phases and the diminishing precipitation hardening effect beyond solubility limits (~5.65 wt% at 548°C). This trade-off between phase connectivity and matrix stiffness highlights the need to balance Cu content to avoid excessive coalescence of Cu-rich phases, which compromises mechanical integrity. The synergistic effect of Al_2O_3 and Cu is most evident in hybrid composites like S2 and S3, where the ceramic particles enhance load transfer and the metallic phases improve stress distribution. The uniform dispersion of Al_2O_3 and controlled distribution of Cu phases in S2 optimize mechanical performance, as evidenced by its superior hardness and elastic modulus.

The elastic-plastic response of the composites, as reflected in the load-displacement curves and plasticity indices, further highlights the influence of microstructure on mechanical behavior. Composites with higher Al_2O_3 content exhibit reduced penetration depths and greater elastic recovery due to the stiffness of the ceramic particles, which resist plastic deformation and enhance the composite's capacity to store elastic energy [60]. In contrast, composites with higher Cu content demonstrate increased plasticity indices, as the ductile nature of Cu allows for greater energy absorption but reduces elastic recovery. This trade-off between stiffness and ductility highlights the importance of tailoring the microstructure to achieve a balance between elastic recovery and plastic deformation.

The wear resistance and frictional behavior of the composites also correlate strongly with their microstructural features. Composites with higher Al_2O_3 content, such as S1 and S2, exhibit superior wear resistance due to the hard ceramic particles acting as barriers to material removal and reducing abrasive wear. In contrast, composites with higher Cu content, such as S4 and S5, show increased wear volume and rates due to the softer nature of Cu, which is more prone to adhesive wear mechanisms. However, the formation of Cu-rich tribolayers in high-Cu composites reduces the coefficient of friction, partially offsetting the increased wear. The tribological data underscores the critical role of Al_2O_3 in maintaining surface integrity and minimizing material loss during sliding, making its presence essential for achieving high wear resistance.

4. Conclusion

This research explored the mechanical properties through nanoindentation, and wear behavior of aluminum-based composites reinforced with different proportions of Al_2O_3 and Cu particles. The following conclusions were drawn:

- The SEM and EDS analyses indicated a uniform dispersion of Al_2O_3 and dendrite like Cu within the aluminum matrix, which contributed to the enhanced mechanical properties of the composites.
- The composite with 7.5 wt% Al_2O_3 and 2.5 wt% Cu exhibited the highest nanohardness and reduced elastic modulus, indicating superior load-carrying capacity and stiffness.
- The penetration depth decreases with Al_2O_3 content contributing to reduction in plasticity index under the applied loads.
- The wear testing demonstrated that the Al_2O_3-reinforced composite had the lowest wear rate, while the composite with 10 wt% Cu also showed competitive wear resistance. This suggests that Al_2O_3 reinforcement significantly enhances wear resistance.
- The combination of 7.5 wt% Al_2O_3 and 2.5 wt% Cu was identified as the optimal reinforcement ratio, providing a balanced enhancement of mechanical strength, stiffness, and wear resistance, making it suitable for applications that require high performance and durability.

CRediT authorship contribution statement

Samuel Ranti Oke: Conceptualization, Investigation, Result analysis, Writing – original draft. **Nthabiseng Maledi:** Resources, Supervision. **Ismail Salaudeen:** Methodology, Writing – review & editing. **Oluwasegun ESo Falodun:** Data analysis.

Declaration of Competing Interest

The authors declare that they have no known competing financial interests or personal relationships that could have appeared to influence the work reported in this paper.

Data Availability

Data will be made available on request.

References

[1] T. Fan, Z. Ruan, F. Zhong, C. Xie, X. Li, D. Chen, P. Tang, Y. Wu, Nucleation and growth of L12-Al3RE particles in aluminum alloys: a first-principles study, J. Rare Earths 41 (2023) 1116–1126.
[2] Q. Hu, W. Liu, Y. Song, H. Li, C. Zhao, M. Xiao, Influence of solid solution treatment on fatigue crack propagation behavior in the thickness direction of 2519A aluminum alloy thick plates, Eng. Fract. Mech. 302 (2024) 110069.
[3] A. Canakcı, S. Ozkaya, F. Erdemir, A.H. Karabacak, M. Celebi, Effects of Fe–Al intermetallic compounds on the wear and corrosion performances of AA2024/316L SS metal/metal composites, J. Alloy. Compd. 845 (2020) 156236.
[4] B.R. Pal, S. Ghosh, P. Sahoo, Aluminium hybrid composites reinforced with SiC and fly ash particles—recent developments, Recent Adv. Layer. Mater. Struct. (2021) 133–170.
[5] S.Ranti Oke, O. Eso Falodun, M.R. Mahlatse, O. Oluremi Ige, P.Apata Olubambi, Investigation on densification and microstructure of Al-TiO2 composite produced by Spark plasma sintering, Mater. Today.: Proc. 18 (2019) 3182–3188.
[6] S.A. Babalola, K.K. Alaneme, S.R. Oke, L.H. Chown, N.B. Maledi, M.O. Bodunrin, Hot compression behaviour and microstructural evolution in aluminium based composites: an assessment of the role of reinforcements and deformation parameters, Manuf. Rev. 8 (2021) 6.
[7] B.S. Babu, P. Prathap, T. Balaji, D. Gowtham, S.S. Adi, R. Divakar, S. Ravichandran, Studies on mechanical properties of aluminum based hybrid metal matrix composites, Mater. Today.: Proc. 33 (2020) 1144–1148.
[8] S. Tang, S. Shao, H. Liu, F. Jiang, D. Fu, H. Zhang, J. Teng, Microstructure and mechanical behaviors of 6061 Al matrix hybrid composites reinforced with SiC and stainless steel particles, Mater. Sci. Eng.: A 804 (2021) 140732.
[9] J. Kumar, D. Singh, N.S. Kalsi, S. Sharma, C.I. Pruncu, D.Y. Pimenov, K.V. Rao, W. Kapłonek, Comparative study on the mechanical, tribological, morphological and structural properties of vortex casting processed, Al–SiC–Cr hybrid metal matrix composites for high strength wear-resistant applications: fabrication and characterizations, J. Mater. Res. Technol. 9 (2020) 13607–13615.
[10] M. Ravikumar, H. Reddappa, R. Suresh, R. Sreenivasa, E. Babu, N. Reddy, C. Ravikumar, H.Ananda Murth, Evaluation of corrosion properties of Al2O3 and SiC reinforced aluminium metal matrix composites using taguchi's techniques, J. Sci. Res. 65 (2021) 253–259.
[11] E. Moustafa, A.M. Khalil, H.M. Ahmed, M. Hefni, A.O. Mosleh, Microstructure, hardness, and wear behavior investigation of the surface nanocomposite metal matrix reinforced by silicon carbide and alumina nanoparticles, J. Miner. Met. Mater. Eng. 7 (2021) 57–62.
[12] S.H. Budapanahalli, S.B. Mallur, A.Y. Patil, A.M. Alosaimi, A. Khan, M.A. Hussein, A.M. Asiri, A tribological study on the effect of reinforcing SiC and Al2O3 in Al7075: applications for spur gears, Metals 12 (2022) 1028.
[13] S.Ranti Oke, O. Eso Falodun, B. Gladness Motsa, O. Oluremi Ige, P. Apata Olubambi, Spark plasma sintering of Al-Ti-Al2O3 composite, Mater. Today.: Proc. 18 (2019) 3946–3951.
[14] A. Sankhla, K.M. Patel, Metal matrix composites fabricated by stir casting process–a review, Adv. Mater. Process. Technol. 8 (2022) 1270–1291.
[15] N. Ahamad, A. Mohammad, K.K. Sadasivuni, P. Gupta, Structural and mechanical characterization of stir cast Al–Al2O3–TiO2 hybrid metal matrix composites, J. Compos. Mater. 54 (2020) 2985–2997.
[16] A.P. Agrawal, S.K. Srivastava, Synthesis, characterization, and mechanical properties of Al–Zn–Mg alloy-based hybrid metal matrix composites reinforced with Si3N4/TiB2 particles processed through stir casting technique, Proc. Inst. Mech. Eng., Part L: J. Mater.: Des. Appl. 238 (2024) 1021–1037.
[17] S.R. Oke, A. Bayode, O.E. Falodun, I.S. Olasupo, Microstructure, mechanical, and wear properties evaluation of Al-Cu based composite using RHA as reinforcement, Can. Metall. Q. (2024) 1–10.
[18] R. Butola, L. Tyagi, R.M. Singari, Q. Murtaza, H. Kumar, D. Nayak, Mechanical and wear performance of Al/SiC surface composite prepared through friction stir processing, Mater. Res. Express 8 (2021) 016520.
[19] T. SuryaKumari, S. Ranganathan, Investigation of Process Parameters on Sliding Wear Behaviour of Aluminium 7075 Hybrid Nanocomposite Analyzed Using Response Surface Methodology-Part I, in: Advances in Materials and Manufacturing Engineering: Select Proceedings of ICMME 2019, Springer, 2021, pp. 461–468.
[20] B. Badhan, H. Nautiyal, R. Moharana, U. Rao, R. Gautam, R. Tyagi, Evaluation of Mechanical Properties and Tribological Behaviour of Self-lubricating Aluminium Matrix Hybrid Composites, in: Recent Advances in Mechanical Engineering: Select Proceedings of ITME 2019, Springer, 2021, pp. 691–698.
[21] V. Vij, R. Agarwal, M.P. Garg, R. Khanna, V. Gupta, Fabrication and mechanical characterization of hybrid composite reinforced with nanoparticles of alumina and zirconia, Polym. Compos. 43 (2022) 7315–7325.
[22] J. Liu, J. Xu, K. Paik, P. He, S. Zhang, In-situ isothermal aging TEM analysis of a micro Cu/ENIG/Sn solder joint for flexible interconnects, J. Mater. Sci. Technol. 169 (2024) 42–52.
[23] M. Gao, P. Gao, Y. Wang, T. Lei, C. Ouyang, Study on metallurgically prepared copper-coated carbon fibers reinforced aluminum matrix composites, Met. Mater. Int. 27 (2021) 5425–5435.
[24] R. Ali, F. Ali, A. Zahoor, R.N. Shahid, T. He, M. Shahzad, Z. Asghar, A. Shah, A. Mahmood, H.B. Awais, Effect of sintering path on the microstructural and mechanical behavior of aluminum matrix composite reinforced with pre-synthesized Al/Cu core-shell particles, J. Alloy. Compd. 889 (2021) 161531.
[25] S. Amirkhanlou, S. Ji, Casting lightweight stiff aluminum alloys: a review, Crit. Rev. Solid State Mater. Sci. 45 (2020) 171–186.
[26] Z. Hu, J. Zheng, L. Hua, Q. Sun, Investigation of forging formability, microstructures and mechanical properties of pre-hardening Al-Zn-Mg-Cu alloy, J. Manuf. Process. 131 (2024) 2082–2100.
[27] O. Akinribide, O. Ogundare, S. Akinwamide, F. Gamaoun, P. Olubambi, Alloying effect of copper in AA-7075 aluminum composite using bale out furnace, J. Mater. Res. Technol. 18 (2022) 3849–3856.
[28] G.B. Rao, P.K. Bannaravuri, R. Raja, K.C. Apparao, P.S. Rao, T.S. Rao, A.K. Birru, R. M.R. Prince, Impact on the microstructure and mechanical properties of Al-4.5 Cu alloy by the addition of MoS2, Int. J. Lightweight Mater. Manuf. 4 (2021) 281–289.
[29] Z. Shen, R. Dong, J. Li, Y. Su, X. Long, Determination of gradient residual stress for elastoplastic materials by nanoindentation, J. Manuf. Process. 109 (2024) 359–366.
[30] X. Long, Y. Li, Z. Shen, Y. Su, T. Gu, K.S. Siow, Review of uniqueness challenge in inverse analysis of nanoindentation, J. Manuf. Process. 131 (2024) 1897–1916.
[31] P. Samal, P.R. Vundavilli, A. Meher, M.M. Mahapatra, Recent progress in aluminum metal matrix composites: A review on processing, mechanical and wear properties, J. Manuf. Process. 59 (2020) 131–152.
[32] P.V. Reddy, G.S. Kumar, D.M. Krishnudu, H.R. Rao, Mechanical and wear performances of aluminium-based metal matrix composites: a review, J. Bio- Tribo-Corros. 6 (2020) 83.
[33] W.C. Oliver, G.M. Pharr, Measurement of hardness and elastic modulus by instrumented indentation: advances in understanding and refinements to methodology, J. Mater. Res. 19 (2004) 3–20.
[34] S.R. Oke, O.E. Falodun, B.G. Motsa, O.O. Ige, P.A. Olubambi, Spark plasma sintering of Al-Ti-Al2O3 composite, Mater. Today.: Proc. 18 (2019) 3946–3951.
[35] J.-q Han, J.-s Wang, M.-s Zhang, K.-m Niu, Relationship between amounts of low-melting-point eutectics and hot tearing susceptibility of ternary Al– Cu– Mg alloys during solidification, Trans. Nonferrous Met. Soc. China 30 (2020) 2311–2325.
[36] M. Ghoncheh, M. Sanjari, A.S. Zoeram, E. Cyr, B.S. Amirkhiz, A. Lloyd, M. Haghshenas, M. Mohammadi, On the microstructure and solidification behavior

of new generation additively manufactured Al-Cu-Mg-Ag-Ti-B alloys, Addit. Manuf. 37 (2021) 101724.
[37] C. Bai, T. Liu, L. Shi, L. Song, Y. Li, R. Su, Y. Zhao, H. Yu, Effect of different Mg2Si concentrations on the wear properties and microstructure of Mg2Si/Al–5 wt% Cu composites, Int. J. Met. (2024) 1–13.
[38] R. Li, G. Ju, X. Zhao, Y. Zhang, Y. Li, G. Hu, M. Yan, Y. Wu, D. Lin, Simulation of residual stress and distortion evolution in dual-robot collaborative wire-arc additive manufactured Al-Cu alloys, Virtual Phys. Prototyp. 19 (2024) e2409390.
[39] Z. Fang, B. Ma, E. Liang, Y. Jia, S. Guan, Interaction regularity of biomolecules on Mg and Mg-based alloy surfaces: a first-principles study, Coatings 14 (2023) 25.
[40] D.-Q. Doan, T.-H. Fang, T.-H. Chen, Interfacial and mechanical characteristics of TiN/Al composites under nanoindentation, Int. J. Solids Struct. 226 (2021) 111083.
[41] S.O. Akinwamide, O.J. Akinribide, P.A. Olubambi, Microstructural evolution, mechanical and nanoindentation studies of stir cast binary and ternary aluminium based composites, J. Alloy. Compd. 850 (2021) 156586.
[42] S.R. Oke, M.R. Mphahlele, O.O. Ige, O.E. Falodun, A.M. Okoro, P.A. Olubambi, Structural characterization and nanoindentation studies on mechanical properties of spark plasma sintered duplex stainless steel nanocomposite, J. Alloy. Compd. 840 (2020) 155648.
[43] Y. Wang, C. Chu, X. Shi, J. Bi, G. Xu, Y. Cao, A. Sun, Microstructure and nanoindentation properties of high-throughput prepared Ti-Al2O3 functionally graded materials films, Mater. Lett. 337 (2023) 133966.
[44] V. Ganesh, R.R. Tamboli, A.K. Khanra, S.R. Dey, Nanoindentation and isothermal compression behaviour of Al–4Cu–Ni composites, Vacuum 225 (2024) 113251.
[45] M. Gao, Z. Chen, L. Li, E. Guo, H. Kang, Y. Xu, T. Wang, Microstructure and enhanced mechanical properties of hybrid-sized B4C particle-reinforced 6061Al matrix composites, Mater. Sci. Eng.: A 802 (2021) 140453.
[46] S. Xu, X. Jing, P. Zhu, H. Jin, K.-W. Paik, P. He, S. Zhang, Equilibrium phase diagram design and structural optimization of SAC/Sn-Pb composite structure solder joint for preferable stress distribution, Mater. Charact. 206 (2023) 113389.
[47] C. Wang, Z. Wang, S. Zhang, X. Liu, J. Tan, Reinforced quantum-behaved particle swarm-optimized neural network for cross-sectional distortion prediction of novel variable-diameter-die-formed metal bent tubes, J. Comput. Des. Eng. 10 (2023) 1060–1079.
[48] A.H. Karabacak, A. Çanakçı, F. Erdemir, S. Özkaya, M. Çelebi, Effect of different reinforcement on the microstructure and mechanical properties of AA2024-based metal matrix nanocomposites, Int. J. Mater. Res. 111 (2020) 416–423.
[49] M. Rezaei, A. Albooyeh, M. Shayestefar, H. Shiraghaei, Microstructural and mechanical properties of a novel Al-based hybrid composite reinforced with metallic glass and ceramic particles, Mater. Sci. Eng.: A 786 (2020) 139440.
[50] B. Sadeghi, P. Cavaliere, A. Perrone, Effect of Al2O3, SiO2 and carbon nanotubes on the microstructural and mechanical behavior of spark plasma sintered aluminum based nanocomposites, Part. Sci. Technol. 38 (2020) 7–14.
[51] A.C. Bhasha, K. Balamurugan, Studies on mechanical properties of Al6061/RHC/TiC hybrid composite, Int. J. Lightweight Mater. Manuf. 4 (2021) 405–415.
[52] M. Dada, P. Popoola, N. Mathe, S. Adeosun, S. Pityana, Investigating the elastic modulus and hardness properties of a high entropy alloy coating using nanoindentation, Int. J. Lightweight Mater. Manuf. 4 (2021) 339–345.
[53] R. Manjunath, D. Kumar, A. Kumar, A review on the significance of hybrid particulate reinforcements on the mechanical and tribological properties of stir-casted aluminum metal matrix composites, J. Bio- Tribo-Corros. 7 (2021) 122.
[54] A.L. Rominiyi, P.M. Mashinini, Nanoindentation study of mechanical and wear properties of spark plasma sintered Ti-6Ni-xTiCN composites, Ceram. Int. 49 (2023) 2194–2203.
[55] Y. Yang, R. Peng, J. Li, X. Chen, H. Zhang, J. Zhao, Y. He, Z. Liu, Elastic-plastic properties of ceramic matrix composites characterization by nanoindentation testing coupled with computer modeling, Ceram. Int. 50 (2024) 18540–18548.
[56] I. Lee, L. Bhatta, Y.-H. Wu, L. Daut, R.B. Figueiredo, K.-D. Liss, B.K. Bay, M. K. Santala, M. Kawasaki, The cold angular rolling process of copper sheets: unraveling plastic deformation behavior and unveiling microstructural transformations, Adv. Eng. Mater. 26 (2024) 2300742.
[57] M.R. Alavandi, J. Haider, D.M. Goudar, Investigation of the influence of Ni and Cu additions on the wear behavior of spray formed Al-15Si alloy at elevated temperature, Silicon 15 (2023) 5963–5980.
[58] V. Bharath, V. Auradi, M. Nagaral, S.B. Boppana, S. Ramesh, K. Palanikumar, Microstructural and wear behavior of Al2014-alumina composites with varying alumina content, Trans. Indian Inst. Met. (2022) 1–15.
[59] E. Mudra, I. Shepa, M. Hrubovcakova, I. Koribanich, D. Medved, A. Kovalcikova, M. Vojtko, J. Dusza, Highly wear-resistant alumina/graphene layered and fiber-reinforced composites, Wear 484 (2021) 204026.
[60] Z. Wang, Y. Ning, P. Di, B. Zhang, H. Yu, B. Xie, Understanding the fracture mechanisms of Ni–Co–Cr-type superalloys: Role of precipitate evolution and strength degradation, Mater. Sci. Eng.: A 902 (2024) 146623.